Optimisation of piezoelectric and dielectric properties of $Bi_4Ti_{2.95}W_{0.05}O_{12}$ ceramics by Ce^{4+} doping

Tao Chen*, Tiantian Liu, Yang Chen, Qi Zhang

School of Electronic Information and Automation, Tianjin University of Science and Technology, Tianjin, 300222, China

Received 16 November 2024; received in revised form 8 March 2025; accepted 11 March 2025

Abstract

High-temperature lead-free $Bi_{4-x}Ce_xTi_{2.95}W_{0.05}O_{12}$ (where x = 0, 0.02, 0.04, 0.06) piezoelectric ceramics were prepared by conventional solid-state method and sintering at 1080 °C. This study investigated the effects of modulating the degree of ceramic lattice distortion by varying the amount of Ce^{4+} doping on the microscopic morphology as well as the piezoelectric and dielectric properties. The results indicated that an appropriate level of Ce^{4+} doping resulted in a suitable degree of lattice distortion within the piezoelectric ceramics, thereby enhancing both the piezoelectric and dielectric properties while reducing dielectric losses. Notably, when the doping level reached x = 0.04, the sample exhibited its optimal performance, specifically with a d_{33} of 25 Pc/N, T_C of 618 °C, tanδ of 0.09 and Q_m of 3364. These findings strongly suggest that this material has significant potential for applications in high-level sensing domain.

Keywords: *Ce-$Bi_4Ti_{2.95}W_{0.05}O_{12}$, lattice distortion, microstructure, dielectric and piezoelectric properties*

I. Introduction

Piezoelectric materials exhibit a unique phenomenon known as the piezoelectric effect, which enables the conversion of electrical energy into mechanical energy and vice versa. This effect allows these materials to undergo mechanical displacement in response to an applied electric field and to generate electrical signals when subjected to mechanical stress. As a result, piezoelectric materials find extensive applications in various fields, including transducers, aerospace technology, electronics and medical devices [1,2].

Bismuth layer-structured ferroelectric materials with general formula $(Bi_2O_2)^{2+}+(A_{m-1}B_mO_{3m+1})^{2-}$ are characterized by high Curie temperature and exceptional thermal stability, which is promising for applications in piezoelectric devices for high-temperature environments [3,4]. Very important representativ of this family is piezoelectric $Bi_4Ti_{2.95}W_{0.05}O_{12}$ (BTW) ceramics. Owing to its distinctive layered structure, the crystal exhibits a relatively elongated *c*-axis, resulting in a substantial coercive field [5,6]. As a result, the polarization process is primarily restricted to the *a*-*b* plane, which makes it difficult to attain a fully polarized state in ceramic materials. From a structural perspective, BTW consists of bismuth oxide layers $(Bi_2O_2)^{2+}$ and perovskite-like layers $(A_{m-1}B_mO_{3m+1})^{2-}$ [7,8]. In bismuth layer-structured piezoelectric ceramics, the bismuth oxide layers act as insulators, while spontaneous polarization predominantly occurs in the perovskite-like layers. Recent studies have indicated that A-site doping exerts a more pronounced effect on enhancing the piezoelectric and ferroelectric properties of these ceramics compared to B-site doping. This disparity is largely attributable to differences in ion size. Cerium (Ce) is commonly employed as an A-site dopant in bismuth layer-structured ferroelectric ceramics, where it typically exists in the +3 and +4 oxidation states. The introduction of Ce doping has been shown to significantly improve the resistivity, temperature stability and piezoelectric performance of these ceramics [9–13].

Although the modification of bismuth-layered piezoelectric ceramics through A-site doping has been extensively studied, the microscopic lattice-level implications remain insufficiently understood. Gaining a deeper understanding of the fundamental mechanisms of doping at this scale is crucial for advancing the development of future piezoelectric materials [14,15]. In this work, the A-sites doping of BTW piezoelectric ceramics with Ce^{4+} ions was investigated and the $Bi_{4-x}Ce_xTi_{2.95}W_{0.05}O_{12}$ (x = 0, 0.02,

*Corresponding author: tel: +86 13716508359
e-mail: *chentao@tust.edu.cn*

0.04, 0.06) ceramics were prepared by the traditional solid-state reaction process and final sintering. This study comprehensively investigates the impact of varying Ce^{4+} doping levels on the lattice distortion of BTW piezoelectric ceramics. Additionally, it examines how these doping variations influence the microscopic morphology, electrical conductivity, piezoelectric performance, dielectric properties and temperature stability of the ceramics.

II. Experimental

$Bi_{4-x}Ce_xTi_{2.95}W_{0.05}O_{12}$ (BCTW, x = 0, 0.02, 0.04, 0.06) ceramic samples were prepared by the conventional solid-state reaction technique. Firstly, raw materials including Bi_2O_3(AR,99%), TiO_2 (AR,99%), WO_3 (AR,99%) and CeO_2 (AR,99%) were weighed according to the stoichiometry. The powders were subjected to ball milling in a planetary ball mill for 16 h by using anhydrous ethanol as the medium and agate balls as the grinding media. The dried powders were subsequently calcined at 800 °C for 4 h in a muffle furnace. The calcined powder was then ball milled for an additional 16 h under identical conditions. After drying, the powders were granulated using 5 wt.% PVA as a binder and subsequently pressed at 300 MPa into disc-shaped slices with a diameter of 15 mm and a thickness of 1 mm. The disc-shaped slices were heated at 650 °C for 2 h to remove the PVA. Subsequently, the slices were sintered in a sealed alumina crucible at 1080 °C for 3 h.

The crystalline phase of the sample was identified by X-ray diffraction (XRD, Model D8 Advanced, Bruker AXS GMBH), the lattice constant of the sample was then obtained by Rietveld refinement fitting. The microstructure was determined by scanning electron microscopy (SEM, Model JSM-6700F).

The sintered ceramics were then polished on both major surfaces and coated with silver paste. The ceramics were then fired at 800 °C for 30 min to form Ag electrodes. For electric measurement, the ceramics were immersed in silicone oil at 150 °C and poled for 30 min under a DC electrical field of 5.5 kV/mm. The temperature dependence of dielectric constant was performed by LCR meter in the temperature range from room temperature to 700 °C (at 0.01–100 kHz). The $d_{33}$was conducted by a piezo-d_{33} meter (ZJ-3A). The mechanical quality factor (Q_m) using an impedance analyser (Agilent 4294A).

III. Results and discussion

3.1. Phase structures

The Raman spectra of BTW-xC ceramics (Fig. 1), measured at ambient temperature, confirmed that high intensity and more pronounced bands occurred at ~94, ~272, ~558 and ~862 cm^{-1}. Compared to the undoped $Bi_4Ti_3O_{12}$-based (BTW) ceramics, the low-frequency Raman peaks of the BTW-xC ceramics with varying doping ratios exhibited significant changes in both peak intensity and frequency position. For bismuth-layered piezoelectric ceramics, the phonon modes can be categorized into low-frequency modes below 200 cm^{-1} and high-frequency modes above 200 cm^{-1}. Among them, the vibration mode around 93 cm^{-1} is associated with the vibrations of Bi^{3+} ions in the bismuth-oxide layers. The mode at 269 cm^{-1} corresponds to the twisting vibration of the TiO_6 octahedra. The modes at around 556 and 863 cm^{-1} are associated with the stretching vibrations of the TiO_6 octahedra. The Raman vibrational modes in the low-frequency region are conventionally linked to lattice vibrations, particularly those associated with ion positions and lattice dynamics. In the case where the substitution of A-site ions leads to lattice compression or a modification of ion-ion interactions, the frequencies of these low-frequency vibrational modes are observed to undergo an increase. This phenomenon referres to as the blue shift phenomenon in Raman spectra. After Ce^{4+} doping at the A-site, the low-frequency Raman peaks of the experimental group exhibit varying degrees of blue shift. This is attributed to the smaller ionic radius of Ce^{4+} replacing the larger Bi^{3+} ion. The smaller ion typically causes a closer arrangement of surrounding oxygen ions and other lattice atoms, leading to lattice distortion, which results in the observed blue shift.

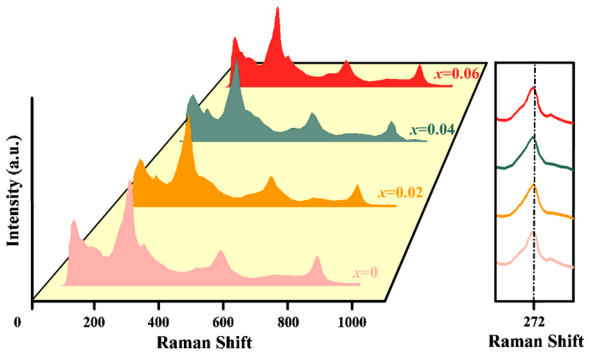

Figure 1. Raman spectra of $Bi_{4-x}Ce_xTi_{2.95}W_{0.05}O_{12}$ ceramics (x = 0, 0.02, 0.04 0.06)

Figure 2 shows the room-temperature XRD pattern of the Ce^{4+} modified $Bi_{4-x}Ce_xTi_{2.95}W_{0.05}O_{12}$ (x = 0, 0.02, 0.03, 0.05) three-layered Aurivillius ceramics. Preliminary XRD analysis confirms the crystallinity and phase purity of the Aurivillius ceramics. The XRD results indicate that the 2θ values and relative peak intensities align well with those specified in the PDF#73-2181 standard card of rhombohedral structure. It is evident that all the ceramics exhibit a bismuth oxide layer-type structure with m = 3 and no

secondary phases are observed within the detected range. The strongest diffraction peak for both the pure and Ce-modified BTW piezoelectric ceramics corresponds to (117) plane and is the highest diffraction peak of bismuth layer-structured materials ($112m$+1). In comparison to the pure BTW ceramics, the intensities of the XRD peaks increase and peak positions of the Ce-modified BTW ceramics exhibit slight shift as shown in Figs. 2a and 2b. This observation indicates that the dopant elements have fully diffused into the lattice, forming a solid solution [16,17]. The observed shift is attributed to the substitution of smaller ionic radius Ce^{4+} (0.97 Å) cations for larger Bi^{3+} (1.03 Å) at varying levels in the A-site of the perovskite-like layers. Such substitution results in varying degrees of distortion within the internal lattice of the ceramics.

The XRD data were analysed by the Rietveld refinement method. Subsequently, the least squares method within the GSAS framework was employed to refine the fitting of the XRD data. The weighted profile R-factor (RWP) values for all samples after refinement consistently remain below 15%, with variance factor JOG values remaining under 2 [18]. These metrics confirm the reliability of our refinement results. Consequently, the lattice parameters presented in Fig. 4 were determined.

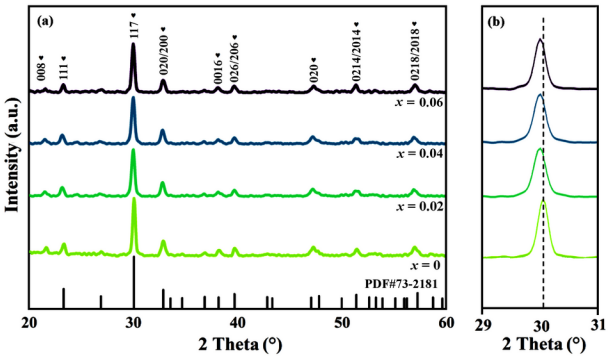

Figure 2. XRD patterns of $Bi_{4-x}Ce_xTi_{2.95}W_{0.05}O_{12}$ ceramics (x = 0, 0.02, 0.04 0.06) at room temperature

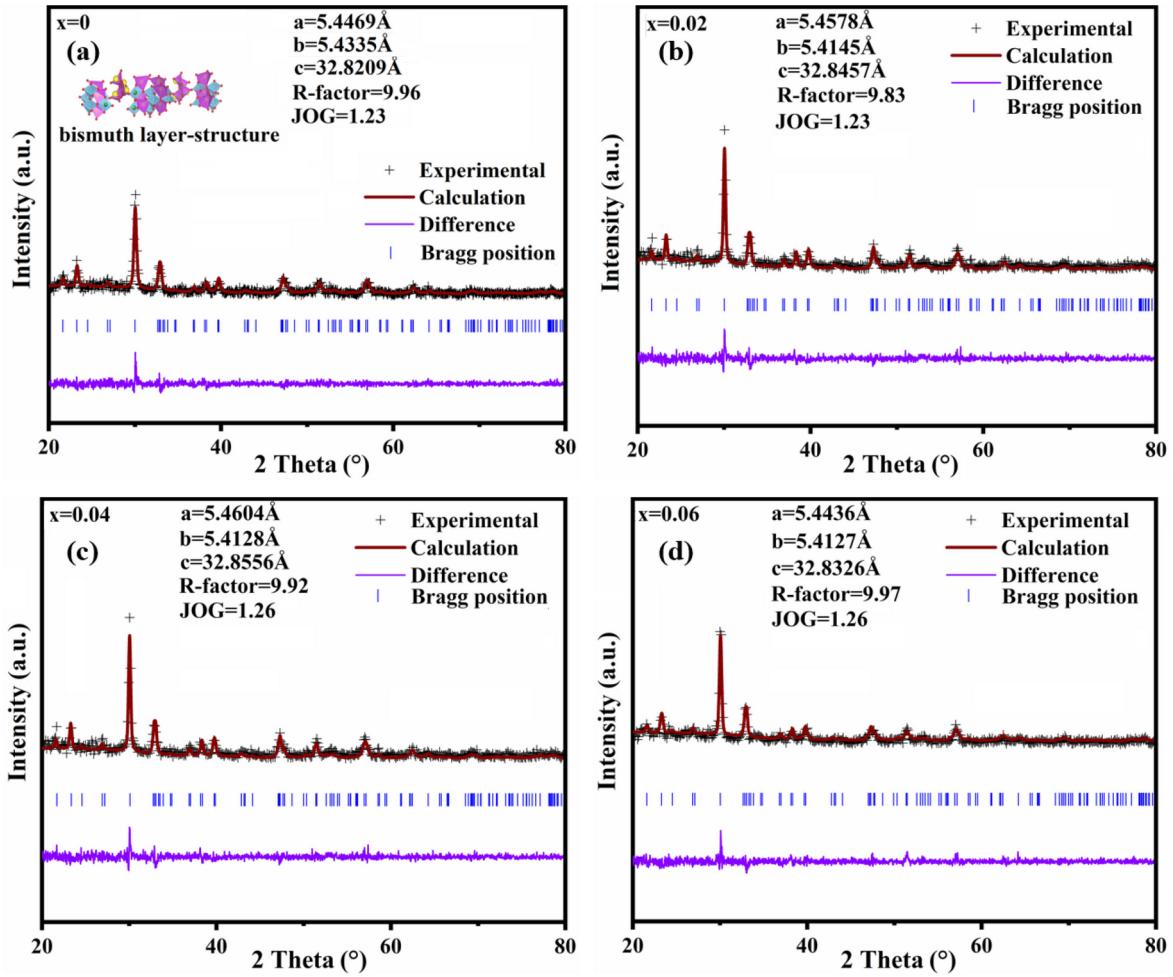

Figure 3. Rietveld profile fits for $Bi_{4-x}Ce_xTi_{2.95}W_{0.05}O_{12}$ ceramics (x = 0, 0.02, 0.04 0.06)

As depicted in Fig. 4, the lattice constants a and c of the ceramics initially increase and then decrease with the increasing Ce^{4+} doping while the trend for b differs. The maximum lattice constants a = 5.4624 Å and c = 32.8588Å are observed at the doping level of x = 0.04, but at this point the value of b is relatively small, b = 5.4178 Å. This phenomenon is likely due to the preferential substitution of atoms along the a and c

axis directions by the doped Ce^{4+} ions, resulting in changes to the lattice constants along these axes. The Ce^{4+} ions, possessing a larger ionic radius, induce lattice expansion upon doping, leading to an increase in the lattice constants *a* and *c* [19–22].

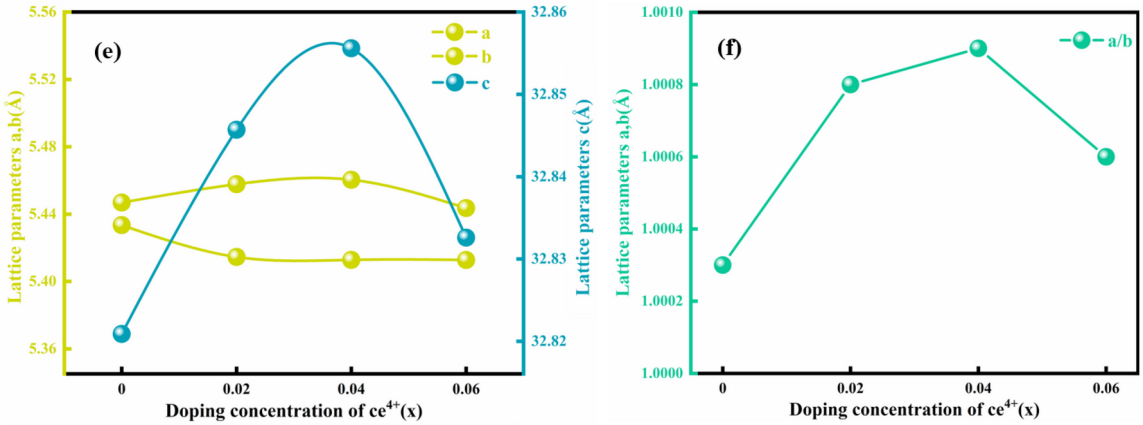

Figure 4. Lattice parameters of $Bi_{4-x}Ce_xTi_{2.95}W_{0.05}O_{12}$ ceramics (x = 0, 0.02, 0.04, 0.06)

The extent of lattice distortion in piezoelectric ceramics is closely associated with their piezoelectric and ferroelectric properties. Variations in lattice distortion exert distinct effects on polarization, piezoelectric coupling and the ferroelectric phase transition of these ceramics. In bismuth layer-structured ferroelectric ceramics, lattice distortion refers to deviations in the atomic arrangement within the internal lattice, arising from variations in atomic size or the presence of structural defects. By modulating atomic doping, it is possible to adjust the degree of lattice distortion, with the aim of optimizing the electronic structure and enhancing polarization strength, thereby improving piezoelectric performance. This strategy has been demonstrated to be effective in optimizing ceramic properties, as evidenced by relevant studies [23–26].

To assess the extent of lateral lattice growth, the rhombohedral distortion index *a*/*b* is commonly used. A larger *a*/*b* value indicates a greater degree of rhombohedral distortion in the ceramics. As shown in Fig. 4, an increase in the *a*/*b* ratio suggests that the doping with Ce^{4+} ions promotes lateral lattice growth and alters the crystal structure and symmetry within the BTW ceramics, introducing anisotropy. This anisotropy can optimize the piezoelectric properties along specific crystal directions, leading to higher piezoelectric coefficients in those directions.

To further analyse the lattice distortion of the BTW-*x*Ce, we selected the (020) crystal planes of four ceramic samples with different doping ratios to calculate the distribution of their charge densities. The structure factors for the samples with varying doping ratios were derived from the refinement results. The charge density distribution for each sample was subsequently calculated using the Fourier inverse transform. The specific formula is provided in the following equation:

$$P(r) = \frac{1}{V}\sum_{h} F(h) \cdot e^{-2\pi i h r} \quad (1)$$

where $P(r)$ represents the electron density at position r, V is the cell volume, $F(h)$ is a structure factor at position h, r denotes a position vector in space, $e^{-2\pi i \cdot h \cdot r}$ is a complex exponential function, $h \cdot r$ represents the dot product of vectors h and r.

Black box lines were used to delineate the atomic lattice, thereby highlighting the extent of lattice distortion within the ceramics at different doping ratios. Since the characteristic crystal plane of all four ceramic samples is (117), which exhibits an orthogonal relationship with the (020) crystal plane, the (020) plane can also provide valuable insight into

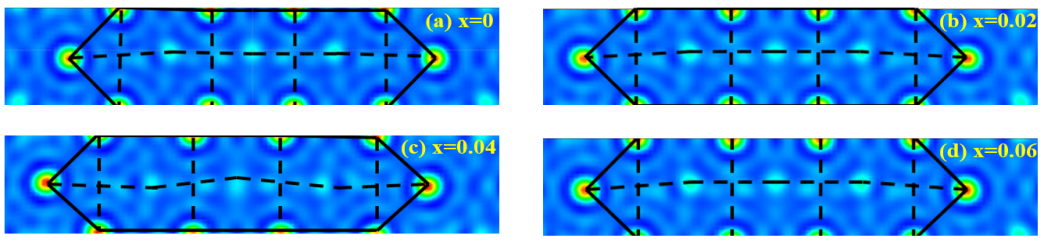

Figure 5. Schematic diagram of charge density on the (020) plane of $Bi_{4-x}Ce_xTi_{2.95}W_{0.05}O_{12}$: a) x = 0, b) x = 0.02, c) x = 0.04 and d) x = 0.06

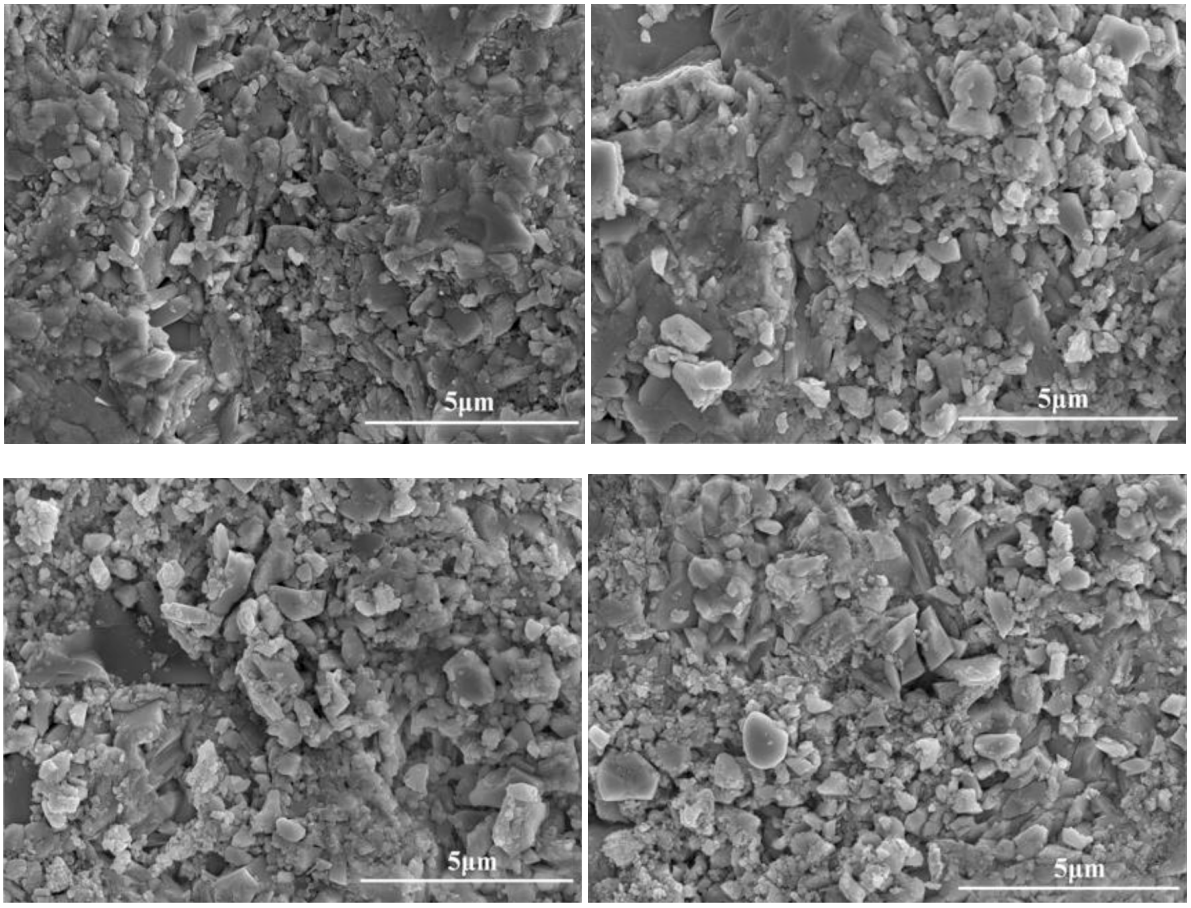

Figure 6. SEM images of $Bi_{4-x}Ce_xTi_{2.95}W_{0.05}O_{12}$: a) $x = 0$, b) $x = 0.02$, c) $x = 0.04$ and d) $x = 0.06$

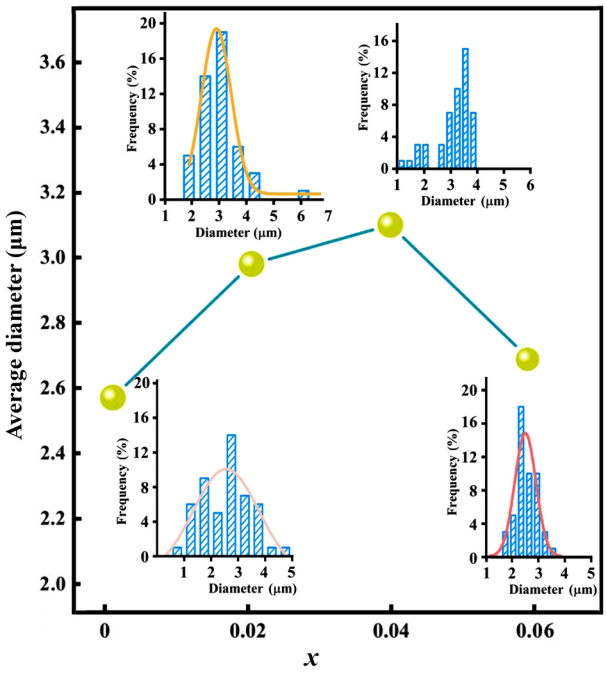

Figure 7. Average grain size and size distribution of $Bi_{4-x}Ce_xTi_{2.95}W_{0.05}O_{12}$ ceramics

the internal lattice distortion within the ceramics [15,26,27]. The charge density distribution of the four samples on the (020) crystal plane is illustrated in Fig. 5. The lattice distortion within the ceramics shows a trend of initially increasing and then decreasing with the doping ratio. The undoped samples exhibit minimal lattice distortion, while the maximum distortion occurs at the doping level of $x = 0.04$.

3.2. Microscopic morphology

Figure 6 presents SEM images of the BTW-*x*Ce ceramics after acid etching. The images clearly illustrates that the grains of BTW bismuth-layered piezoelectric ceramics exhibit pronounced anisotropy in their growth direction. This characteristic is attributed to the accelerated growth rate of the bismuth-layered piezoceramic grains along the *c*-axis of the crystal, leading to the formation of a typical plate-like structure in all samples [28].

A total of fifty random grain size measurements were taken for each sample using the Nano Measurer software to generate a grain size distribution map and calculate the average grain size. The results indicate that as the doping level gradually increases, the surface of the ceramics becomes denser, the grain size becomes more uniform and the anisotropy is significantly reduced (Fig. 6). Notably, the grain size initially exhibits an upward trend, followed by a gradual decline (Fig. 7). This behaviour can be attributed to the tendency of Bi in BTW ceramics to

form bismuth oxides at elevated temperatures, which subsequently volatilize and generate an increase in cationic vacancies. The expansion of defect vacancies within the ceramics is detrimental to grain growth, as illustrated by Eqs. 2 and 3. The doping of Ce^{4+} can replaces a portion of the Bi^{3+} element, thereby indirectly reducing the formation of defective vacancies in the ceramics, as shown in Eq. 4. At lower Ce^{4+} doping levels, the dopant element replaces Bi^{3+} in the perovskite-like layers away from the A-site, inducing lattice distortion. This distortion alleviates localized stress concentrations within the ceramic and creates favourable energy conditions. The regions of lattice distortion exhibit lower energy barriers, facilitating the movement of atoms or ions, thereby promoting easier grain growth. However, when Ce^{4+} doping becomes excessive, the densification of the ceramic surface diminishes and the grain size is reduced. This phenomenon is primarily attributed to the accumulation of excess Ce^{4+}at grain boundaries, which impedes grain growth.

$$Bi_2O_3 \xrightarrow{\Delta} 2Bi(gas)\uparrow+3/2\ O_2(gas)\uparrow+2V'''_{Si}+3V_O^{\bullet\bullet} \quad (2)$$

$$1/2O_2+ V_O^{\bullet\bullet} \rightarrow O_O^X+2h^{\bullet} \quad (3)$$

$$2CeO_2 \xrightarrow{Bi_2O_3} 2Ce_{Bi}+1/2O_2(gas)\uparrow+2e' \quad (4)$$

The bulk densities of the sintered samples were determined using the Archimedean method and presented in Fig. 8. The results reveal a non-monotonic trend, with bulk density first increasing and then decreasing, reaching its maximum at x = 0.02. It is believed that doping with Ce^{4+} reduces the volatilization of Bi at elevated temperatures and enhancing the bulk density. However, as the doping concentration increases further, the bulk density decreases due to an increase in lattice distortion. This distortion may induce lattice stress, hindering atomic diffusion during the sintering process, which in turn leads to a reduction in bulk density.

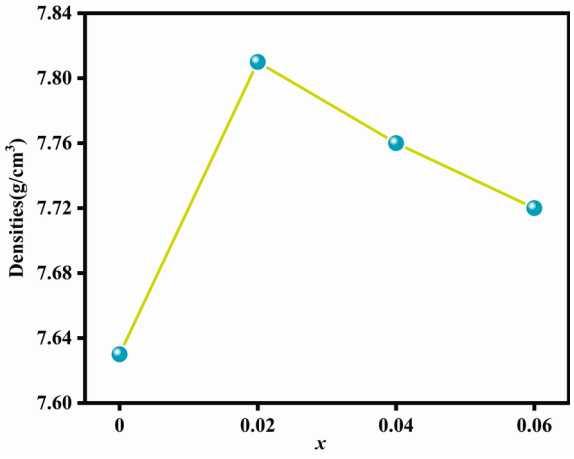

Figure 8. Bulk densities of $Bi_{4-x}CexTi_{2.95}W_{0.05}O_{12}$ ceramics

3.3. Dielectric properties

Figure 9 illustrates the temperature dependence of the dielectric properties of the BTW-*x*Ce ceramics measured at various frequencies. As it can be seen, the temperature at which the peak of the dielectric constant versus temperature curve occurs is identified as the Curie temperature (T_C). The Curie temperature marks the onset of the phase transition, which, in BTW ceramics, signifies the transition from the ferroelectric rhombohedral phase to the paraelectric tetragonal phase. At frequencies of 0.1, 1, 10 and 100 kHz, all samples exhibit a pronounced permittivity peak in the ε_r-T curves around 630 °C. The consistency of these permittivity peak positions across different frequencies indicates that the BTW-*x*Ce ceramics undergo a typical phase transition from the ferroelectric to the paraelectric state at this characteristic temperature.

The Curie temperature of the undoped pure BTW ceramics is 628 °C. As the doping level increases, the Curie temperature initially decreases before rising again. The lowest observed Curie temperature, 618 °C, occurs at a doping concentration of x = 0.04. For doping amounts of x = 0.02 and x = 0.06, the Curie temperatures are 620 and 622°C, respectively (Fig. 9). This behaviour is closely related to the degree of lattice distortion within the piezoelectric ceramics. The relationship between lattice distortion and the Curie temperature can be evaluated using the tolerance factor t. This factor is commonly used to describe the stability of the lattice structure and the degree of geometric compatibility between the ions, which indirectly reflects the extent of internal lattice distortion, as illustrated in Eq. 5:

$$t = \frac{R_A + R_O}{\sqrt{2(R_B + R_O)}} \quad (5)$$

where R_A is the ionic radius of the A-site cation, R_B is the ionic radius of the B-site cation, and R_O is the ionic radius of the oxyanion.

The greater the deviation of the tolerance factor from 1, the more pronounced the lattice distortion becomes. Lattice distortion leads to in increased stresses and defects within the lattice, rendering the lattice structure unstable and causing a reduction in the temperature at which the ferroelectric phase transitions to the paraelectric phase, known as the Curie temperature [29].

In bismuth layer-structured ferroelectric ceramics, internal lattice distortion primarily arises from the mismatch between the bismuth oxide layers and the perovskite-like layers. Specifically, the Bi^{3+} ions in the bismuth-oxygen layer are “under-bonded”, while the A-site cations in the perovskite like layers are “over-bonded”. The coexistence of these bonding states contributes to the stabilization of their structure [30]. Upon doping with Ce^{4+}, the concentration of defects,

such as oxygen vacancies, within the ceramics is reduced. Additionally, the dopant ions can enter the bismuth oxide layers, mitigating the "under-bonded" of the Bi^{3+} ions while increasing the "over-bonded" of the A-site cations in the perovskite-like layers. However, due to the differences in valence and ionic radius between the dopant and the host ions, this doping behaviour can further intensify the degree of lattice distortion within BTW ceramics, consequently leading to decrease in the Curie temperature. The relative permittivity of the doped ceramic samples is significantly elevated. This phenomenon can be attributed to the introduction of higher valence cations at the A-site through doping substitution, which increases the number of excess electrons within the ceramics. Consequently, a greater number of free electrons are excited in the high-temperature region, which in turn can induce additional charges, thereby effectively increasing the relative permittivity of the ceramics.

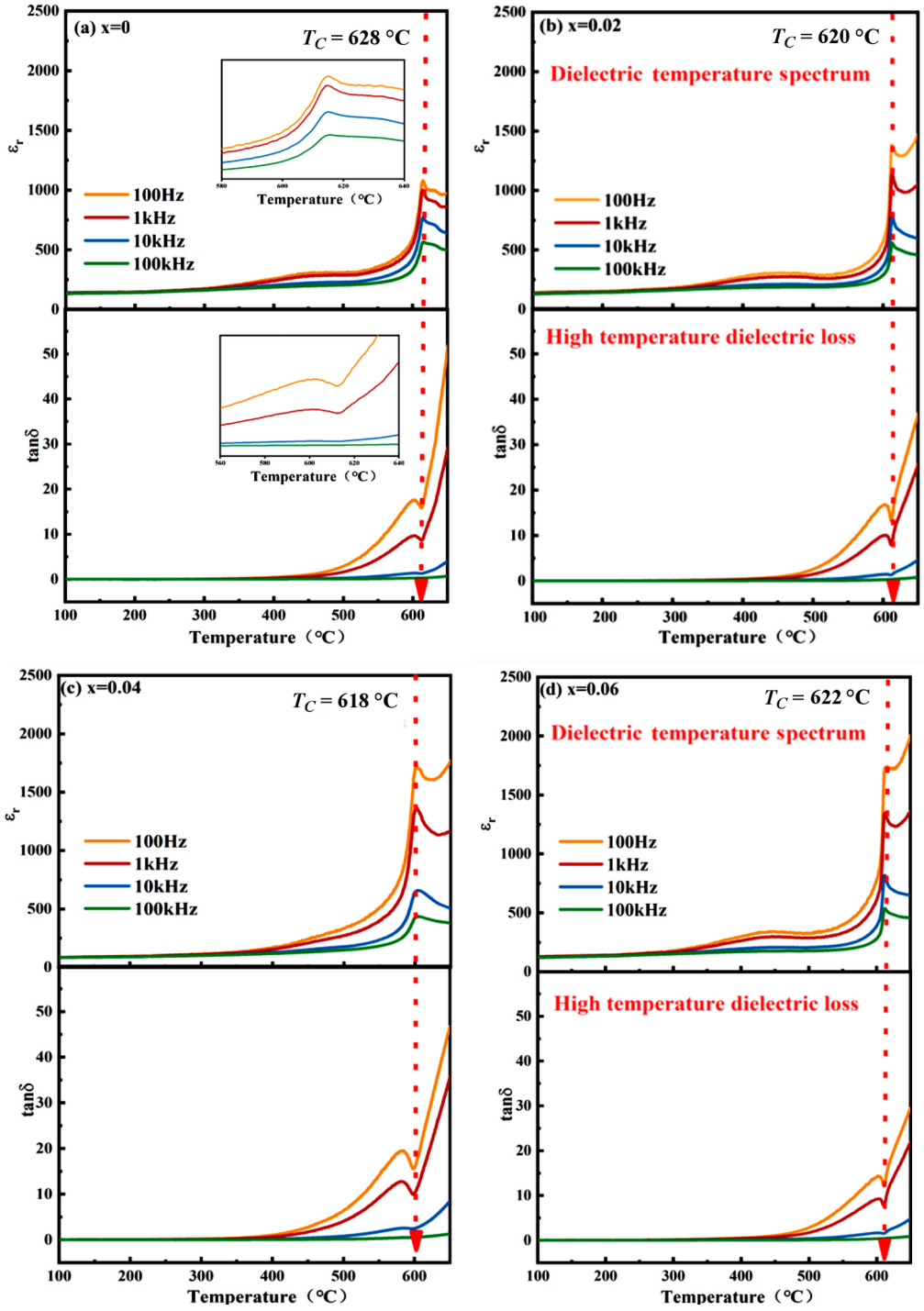

Figure 9. Temperature dependence of dielectric properties of $Bi_{4-x}Ce_xTi_{2.95}W_{0.05}O_{12}$ measured at different frequencies: a) x = 0, b) x = 0.02, c) x = 0.04 and d) x = 0.06

The dielectric loss in bismuth layer-structured ferroelectric materials arises from energy dissipation during the movement of electrical domains and the reorientation of spontaneous polarization. This energy dissipation is primarily due to the frictional resistance encountered by domain wall motion as it interacts with the internal defects of the material. Across all ceramic samples, the dielectric loss remained relatively stable from room temperature up to approximately 450 °C. However, a marked increase in dielectric loss was observed in all samples when the temperature exceeded 450 °C, a phenomenon attributed to a significant rise in leakage current at elevated temperatures [31,32]. The intensity of the dielectric loss peaks in the ceramic samples exhibited a dual trend with respect to doping levels. Initially, the peak dielectric loss decreased with increasing doping, followed by a gradual increase. Notably, the undoped sample exhibited the highest peak dielectric loss, while the sample with a doping level of x = 0.04 showed the lowest peak dielectric loss.

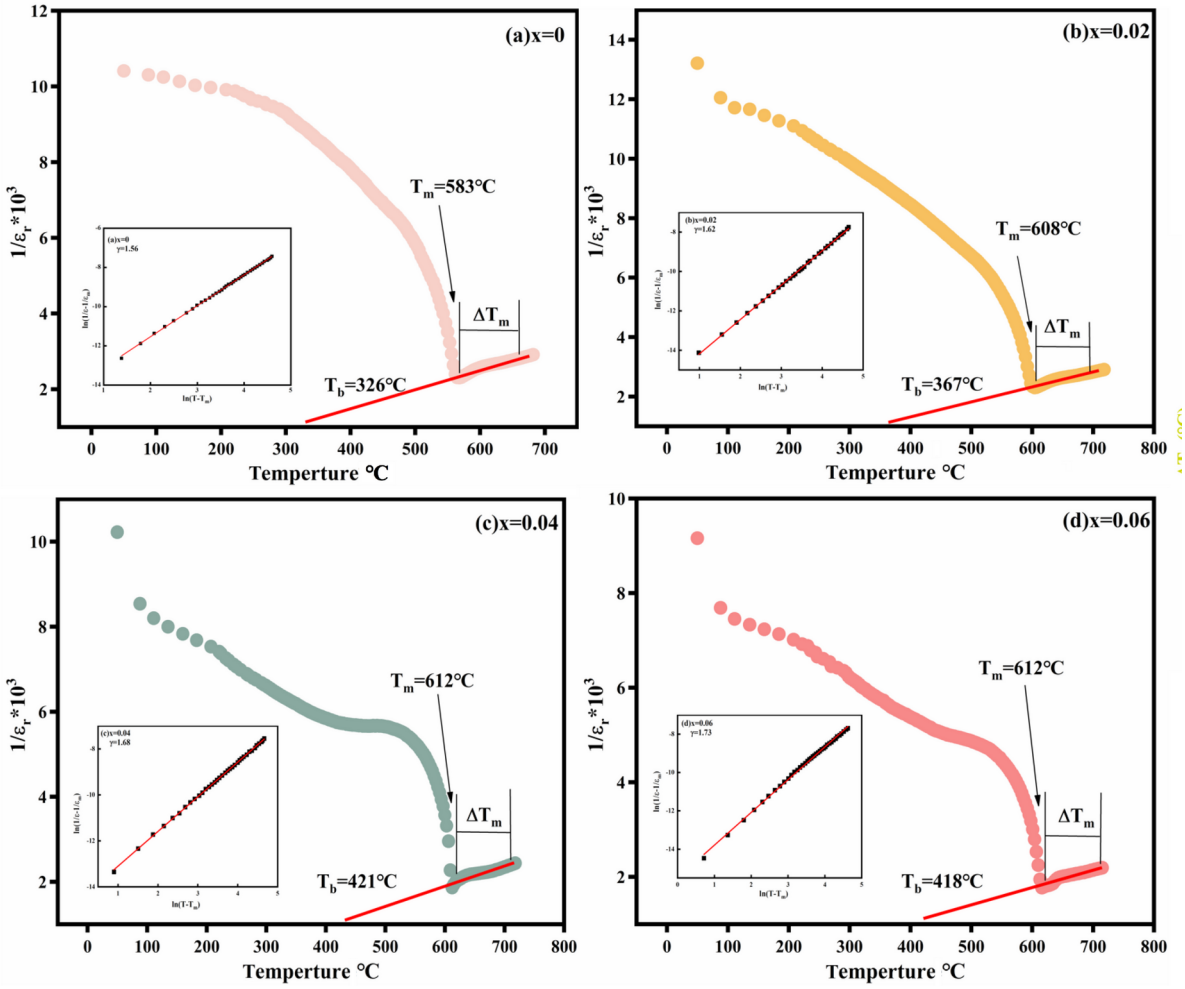

Figure 10. (a)-(d) The inverse dielectric constant at 100 kHz as a function of temperature for the BTW-*x*Ce ceramic samples (insets are corresponding curves of $\ln(1/\varepsilon - 1/\varepsilon_m)/\ln(T-T_m)$ at 100 kHz)

The reduction in the intensity of the dielectric loss peak can be attributed to moderate Ce^{4+} doping, which induces a controlled lattice distortion. This distortion decreases the concentration of oxygen vacancies generated by the volatilization of the Bi^{3+} element, thereby diminishing the pinning effect of these defective vacancies on the electrical domains. Consequently, the electrical domains within the ceramics become more closely arranged, resulting in reduced friction and loss. However, when the doping concentration was further increased to x = 0.06, the intensity of the dielectric loss peak exhibited a rebound. This phenomenon is likely due to the introduction of new defects, such as dislocations, caused by excessive doping. These defects amplify the pinning effect of the vacancies on the electrical domains, leading to increased dielectric loss values in the samples [33]. Figure 10 illustrates relationship between the inverse dielectric constant and temperature for the BTW-*x*Ce ceramic samples at a frequency of 100 kHz. When the testing temperature exceeds the Curie temperature (T_C) of each ceramic

composition, the inverse of the dielectric constant for a typical ferroelectric material is expected to follow the Curie-Weiss law (for $T > T_m$), as expressed by the equation:

$$\frac{1}{\varepsilon} = \frac{T - T_{CW}}{C} \quad (6)$$

where C represents the Curie-Weiss constant and T_{CW} is the Curie-Weiss temperature, which can be obtained by fitting the above equation. These curves deviate from the Curie-Weiss law, and the degree of deviation is defined as $\Delta T_m = T_b - T_m$. T_b is the starting temperature at which the dielectric constant begins to follow the Curie-Weiss law, and T_m is the temperature at which the dielectric constant reaches its maximum value. Initially, the T_m value increases with increasing Ce^{4+} doping concentration, but then decreases. The trend of the dielectric constant temperature (ΔT_m) is consistent with the degree of diffusive phase transition. The variation in diffuseness is attributed to the lattice distortion and the change in the number of defect dipoles induced by Ce ion doping in BTW ceramics. The maximum of the temperature-dependent dielectric constant (ΔT_m) value is observed at $x = 0.04$, corresponding to the point at which the dielectric relaxation behaviour of the ceramic samples is most pronounced. For relaxor ferroelectrics, the relationship between the inverse dielectric constant and temperature is described by the modified Curie-Weiss law, as demonstrated in the following equation:

$$\frac{1}{\varepsilon} - \frac{1}{\varepsilon_m} = \frac{T - T_m}{C}\gamma \quad (7)$$

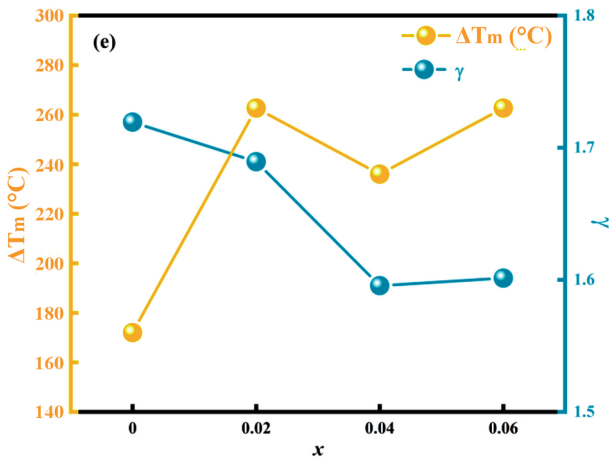

Figure 11. Changes in ΔT_m and γ of BTW-xCe ceramic samples

Here, ε_m is the peak dielectric constant, T_m is the temperature corresponding to the maximum dielectric constant, C is the Curie constant and γ is the diffuseness coefficient, with a value range of $1 < \gamma < 2$, indicating that the ceramic samples are relaxor ferroelectrics. The insets in Fig. 10 show the relationship between $\ln(1/\varepsilon - 1/\varepsilon_m)$ and $\ln(T - T_m)$ at 100 kHz, from which the value of the diffuseness coefficient γ can be defined by the slope. The corresponding values are given in Fig. 11. The dielectric relaxation behaviour in relaxor ferroelectrics can be explained by the concepts of superparaelectricity and superferroelectricity. Due to the A-site doping by higher-valence Ce^{4+}, lattice distortion, and charge imbalance occur in the perovskite-like layered structure, leading to the formation of polar nanoregions in all sample compositions, which promotes dielectric relaxation behaviour. Therefore, piezoelectric ceramics with pronounced relaxation behaviour can enhance their electrical properties.

3.4. Piezoelectric properties

Figure 12a illustrates the variation in the piezoelectric properties of the BTW ceramics with different doping amounts of Ce^{4+}. It is evident that the piezoelectric coefficient of the ceramics reaches a maximum d_{33} of 25 pC/N at a doping amount of $x = 0.04$, which is three times that of the undoped pure BTW ceramics (8 pC/N). This indicates a significant enhancement in the piezoelectric properties of the ceramics with Ce^{4+} doping. The enhancement in piezoelectric properties arises from the intrinsic nature of piezoelectricity, which is based on the asymmetry of positive and negative charges within the crystal. Substituting Bi^{3+} with Ce^{4+} ions further accentuates this asymmetry by inducing lattice distortion, thereby increasing the piezoelectric coefficient. An increase in structural asymmetry amplifies the relative displacements between ions in ceramic materials, particularly between cations and anions. This displacement enhances the material's polarization strength, thereby improving its piezoelectric coefficient. The introduction of lattice distortion generates internal stresses, which modify the local electric field distribution and facilitate domain wall motion. Moderate levels of internal stress can enhance domain wall mobility, leading to an improvement in the piezoelectric properties. However, the piezoelectric coefficient decreased to 18 pC/N when the doping amount was increased to $x = 0.06$. This reduction is primarily attributed to excessive doping, which leads to an increase in the concentration of defects and vacancies within the ceramics. Consequently, the number of switched electric domain walls within the ceramics is reduced. Concurrently, the pinning effect on the electric domains is augmented, impairing the reorientation of the electric domains during the polarization process and rendering the polarization inadequate. This ultimately results in a decline in the piezoelectric properties [31].

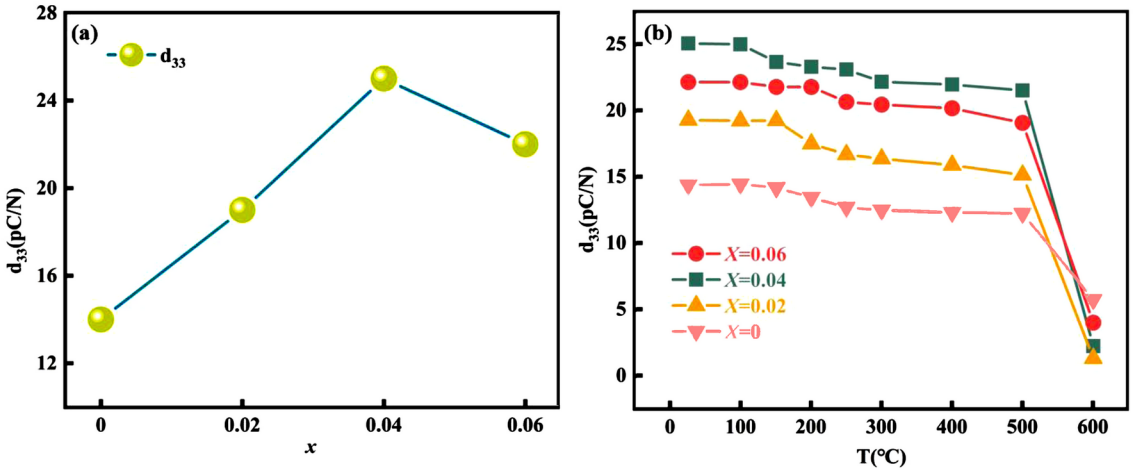

Figure 12. The d_{33} of BTW-xCe ceramics at room temperature (a) and the d_{33} of BTW-xCe ceramics at different temperatures (b)

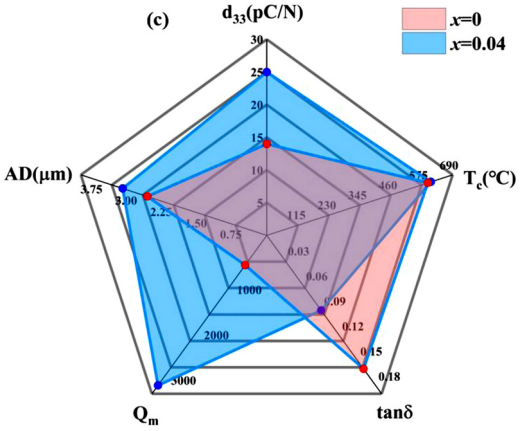

Figure 13. Radar analysis plots of BTW ceramics for x =0 and x = 0.04

Figure 12b illustrates the relationship between the d_{33} and depolarization temperature curves for the BTW-xCe ceramics. For each temperature point in the temperature-dependent test, the ceramics were maintained at the set temperature for 30 min, and the d_{33} piezoelectric coefficient was measured for each ceramic composition at that temperature. As it is shown in Fig. 12, the d_{33} values of all experimental groups remain relatively stable with only a small variation below 500 °C, and the ceramics with x = 0.04 doping exhibit superior temperature stability. Above 500 °C, the d_{33} values of the ceramics decrease sharply, reaching only about 13% of the room temperature value.

Figure 13 presents a comparative analysis of the properties of the undoped BTW and doped BTW (with x = 0.04) ceramics. All properties of the doped BTW (with x = 0.04) sample exhibit marked improvement in comparison to those of the undoped BTW sample. Among the observed changes, the d_{33}, Q_m and average diameter exhibited notable increases, from 14 pC/N, 658, 2.57 μm to 25 pC/N, 3314, 3.1 μm, respectively. Furthermore, the tanδ value decreased from 0.16 to 0.09. In conclusion, the doped BTW with 4 at.% Ce ceramics has the potential to be utilized in applications at high temperatures.

IV. Conclusions

$Bi_{4-x}Ce_xTi_{2.95}W_{0.05}O_{12}$ (BCTW, x = 0, 0.02, 0.04, 0.06) ceramics samples were prepared by the conventional solid-state reaction technique and sintering at 1080 °C. The doping with Ce^{4+} into the pristine ceramic formulation was performed to modulate the degree of lattice distortion. The resulting doped ceramics were thoroughly examined, focusing on their micro-morphology as well as their piezoelectric and dielectric properties. This investigation led to the following conclusions:

1. All the prepared ceramic samples exhibited a bismuth layered structure with m = 3. A detailed analysis of the lattice parameters enabled the calculation of the rhombohedral distortion index, demonstrating that the degree of lattice distortion in piezoelectric ceramics can be effectively regulated through the introduction of Ce^{4+}.
2. The doping of Ce^{4+} elements facilitates enhanced grain growth by increasing the degree of lattice distortion in the ceramics. This process not only improves the surface density of the ceramics but also significantly enhances their piezoelectric properties.
3. Doping with elemental Ce^{4+} enhances the degree of lattice distortion in the ceramics, which further reduces defects and vacancies. This reduction weakens the pinning effect of the internal domains, thereby significantly improving the dielectric properties of the ceramics.

References

1. T. Zheng, J. Wu, D. Xiao, "Recent development in lead-free perovskite piezoelectric bulk materials", *Prog. Mater. Sci*., 2018, **98** (2018) 552–624.
2. S. Zhang, F. Yu, "Piezoelectric materials for high temperature sensors", *J. Am. Ceram. Soc*., **94** [10] (2011) 3153–3170.
3. A. Moure, A. Castro, L. Pardo, "Aurivillius-type ceramics, a class of high temperature piezoelectric materials: Drawbacks, advantages and trends", *Prog. Solid State Chem*., **37** [1] (2009) 15–39.
4. T. Stevenson, D.G. Martin, P.I. Cowin, "Piezoelectric materials for high temperature transducers and actuators", *J. Mater. Sci.: Mater. Electron*., **26** (2015) 9256–9267.
5. A. Peláiz-Barranco, Y. González-Abreu, "Ferroelectric ceramic materials of the Aurivillius family", *J. Adv. Dielectr.*, **3** [4] (2013) 1330003.
6. X.C Xie, Z.Y. Zhou, R.H. Liang, X.L. Dong, "Superior piezoelectricity in bismuth titanate-based lead-free high-temperature piezoceramics via domain engineering", *Adv. Electron. Mater*., **8** [7] (2022) 2101266.
7. M. Takahashi, Y. Noguchi, M. Miyayama, "Effects of V-doping on mixed conduction properties of bismuth titanate single crystals", *Jpn. J. Appl. Phys*., **42** [9S (2003) 6222.
8. R.L. Withers, J.G. Thompson, A.D. Rae, "The crystal chemistry underlying ferroelectricity in $Bi_4Ti_3O_{12}$, Bi_3TiNbO_9, and Bi_2WO_6", *J. Solid State Chem*., **94** [2] (1991) 404–417.
9. Q. Zhang, Y. Zhang, H. Sun, Q. Sun, X. Wang, X. Hao, S. An, "Photoluminescence, photochromism, and reversible luminescence modulation behavior of Sm-doped $Na_{0.5}Bi_{2.5}Nb_2O_9$ ferroelectrics", *J. Eur. Ceram. Soc*., **37** [3] (2017) 955–966.
10. J.N. Chen, Q. Wang, H.T. Lu, et al., "Enhanced electrical properties and conduction mechanism of A-site rare-earth Nd-substituted $CaBi_2Nb_2O_9$", *J. Phys. D: Appl. Phys*., **55** [31] (2022) 315301.
11. J. Hou, R.V. Kumar, Y. Qu, D. Krsmanovic, "B-site doping effect on electrical properties of $Bi_4Ti_{3-2x}Nb_xTa_xO_{12}$ ceramics", *Scripta Mater*., **61** [6] (2009) 664–667.
12. Z.G. Gai, M.L. Zhao, W.B. Su, et al. "Influences of ScTa co-substitution on the properties of Ultra-high temperature Bi_3TiNbO_9-based piezoelectric ceramics", *J. Electroceram*., **31** (2013) 143–147.
13. J. Hou, Y. Qu, R. Vaish, K.B.R. Varma, D. Krsmanovic, R. Vasant Kumar, "Crystallographic evolution, dielectric, and piezoelectric properties of $Bi_4Ti_3O_{12}$: W/Cr ceramics", *J. Am. Ceram. Soc*., **93** [5] (2010) 1414–1421.
14. T. Sivakumar, M. Itoh, "Ferroelectric phase transitions in new Aurivillius oxides: $Bi_{2+2x}Sr_{1-2x}Nb_{2-x}Sc_xO_9$", *J. Mater. Chem*., **21** [29] (2011) 10865–10870.
15. H. Yan, Z. Zhang, W. Zhu, L. He, Y. Yu, C. Li, J. Zhou, "The effect of (Li,Ce) and (K,Ce) doping in Aurivillius phase material $CaBi_4Ti_4O_{15}$", *Mater. Res. Bull*., **39** [9] (2004) 1237–1246.
16. F. Rehman, J.-B. Li, M.-S. Cao, Y.-J. Zhao, M. Rizwan, H.-B. Jin, "Contribution of grains and grain boundaries to dielectric relaxations and conduction of Aurivillius $Bi_4Ti_2Fe_{0.5}Nb_{0.5}O_{12}$ ceramics", *Ceram. Int*., **41** [10] (2015) 14652–14659.
17. C.-M. Wang, J.-F. Wang, C. Mao, X. Chen, X. Dong, Z.-G. Gai, M.-L. Zao, "Enhanced dielectric and piezoelectric properties of aurivillius-type potassium bismuth titanate ceramics by cerium modification", *J. Am. Ceram. Soc*., **91** [9] (2008) 3094–3097.
18. A. Kumar, D. Varshney, ",Crystal structure refinement of $Bi_{1-x}Nd_xFeO_3$ multiferroic by the Rietveld method", *Ceram. Int*., **38** [5] (2012) 3935–3942.
19. V. Shrivastava, A.K. Jha, R.G.. Mendiratta, "Dielectric studies of La and Pb doped $SrBi_2Nb_2O_9$ ferroelectric ceramic", *Mater. Lett*., **60** [12] (2006) 1459–1462.
20. C.L. Diao, J.B. Xu, H.W. Zheng, L. Fabg, Y.Z. Gu, W.F. Zhang, "Dielectric and piezoelectric properties of cerium modified $BaBi_4Ti_4O_{15}$ ceramics", *Ceram. Int*., **39** [6] (2013) 6991–6995.
21. Y. Shimakawa, Y. Kubo, Y. Nakagawa, et al., "Crystal structures and ferroelectric properties of $SrBi_2Ta_2O_9$ and $Sr_{0.8}Bi_{2.2}Ta_2O_9$", *Appl. Phys. Lett*., **74** [13] (1999) 1904–1906.
22. Y. Shimakawa, Y. Kubo, Y. Nakagawa, S. Goto, T. Kamiyama, H. Asano, F. Izumi, "Crystal structure and ferroelectric properties of $ABi_2Ta_2O_9$ (A= Ca, Sr, and Ba)", *Phys. Rev. B*, **61** [10] (2000) 6559.
23. G. Liu, C. Wu, Y. Chen, D. Liang, B. Wang, J. Wu, Q. Chen, "Enhanced ferroelectricity of $CaBi_2Nb_2O_9$-based high-temperature piezoceramics by pseudo-tetragonal distortion", *Ceram. Int*., **44** [6] (2018) 5880–5885.
24. X.X. Tian, S.B. Qu, H.L. Du, et al., "Effects of (LiCe) co-substitution on the structural and electrical properties of $CaBi_2Nb_2O_9$ ceramics", *Chin. Phys. B*, **21** [3] (2012) 037701.
25. X. Xie, Z. Zhou, T. Chen, R. Liang, X. Dong, "Enhanced electrical properties of NaBi modified $CaBi_2Nb_2O_9$-based Aurivillius piezoceramics via structural distortion", *Ceram. Int*., **45** [5] (2019) 5425–5430.
26. C.-M. Wang, J.-F. Wang, S. Zhang, T.R. Shrout, "Electromechanical properties of A-site (LiCe)-modified sodium bismuth titanate ($Na_{0.5}Bi_{4.5}Ti_4O_{15}$) piezoelectric ceramics at elevated temperature", *J. Appl. Phys*., **105** [9] (2009) 094110.
27. X.C. Xie, Z.Y. Zhou, T. Chen, R.H. Liang, X.L. Dong, "Enhanced electrical properties of NaBi modified $CaBi_2Nb_2O_9$-based Aurivillius piezoceramics via structural distortion", *Ceram. Int*., **45** [5] (2019) 5425–5430.
28. Q.Q. Hou, B. Yang, C. Ma, Z.Y. Zhou, R.H. Liang H. Li, X.L. Dong, "Tailoring structure and piezoelectric properties of $CaBi_2Nb_2O_9$ ceramics by W^{6+}-doping", *Ceram. Int*., **48** [12] (2022) 16677–16684.
29. X. Xie, Z. Zhou, R. Liang, et al., "Superior piezoelectricity in bismuth titanate-based lead-free high-temperature piezoceramics via domain engineering", *Adv. Electron. Mater*., **8** [7] (2022) 2101266.
30. S.M. Blake, "Cation disorder in ferroelectric Aurivillius phases of the type $Bi_2ANb_2O_9$ (A= Ba, Sr, Ca)", *J. Mater. Chem*., **7** [8] (1997) 1609–1613.
31. C. Long, B. Wang, W. Ren, K. Zheng, H. Fan, D. Wang, L. Liu, "Significantly enhanced electrical properties in $CaBi_2Nb_2O_9$-based high-temperature

piezoelectric ceramics", *Appl. Phys. Lett*., **117** [3] (2020) 032902.

32. G. Liu, D. Wang, C. Wu, J. Wu, Q. Chen, "A realization of excellent piezoelectricity and good thermal stability in $CaBi_2Nb_2O_9$: Pseudo phase boundary", *J. Am. Ceram. Soc*., **102** [4] (2019) 1794–1804.

33. O. Bidault, P. Goux, M. Kchikech, et al., "Space-charge relaxation in perovskites", *Phys. Rev. B*, **49** [12] (1994) 7868.